ACS APPLIED BIO MATERIALS

www.acsabm.org Article

Transfection of Unmodified MicroRNA Using Monolayer-Coated Au Nanoparticles as Gene-Delivery Vehicles

Johnson Hoang, Sagar L. Patil, Pannaree Srinoi, Tingting Liu, Maria D. Marquez, Orawan Khantamat, Wirote Tuntiwechapikul, Preethi H. Gunaratne,* and T. Randall Lee*

Cite This: *ACS Appl. Bio Mater.* 2024, 7, 230−237 Read Online

ACCESS | Metrics & More | Article Recommendations | Supporting Information

ABSTRACT: This article describes a monolayer-coated gold nanoparticle-based transfection system for the delivery of microRNA (miRNA) into human osteosarcoma (HOS) cells. Two distinct ammonium-terminated adsorbates were used in this study, which provided a platform for ionic bonding of the miRNA onto gold nanoparticles (AuNPs). The custom-designed monolayer-coated gold nanoparticles were characterized by dynamic light scattering, gel mobility shift assay, transmission electron microscopy, ultraviolet−visible spectrometry, zeta potential, and X-ray photoelectron spectroscopy. The miRNA-loaded gold nanoparticles were transfected, and the level of intracellular miRNA delivered and taken up by cells was measured by Taqman qPCR. The overall analysis indicated a successful delivery of miRNA into the HOS cells at an ∼11,000-fold increase compared to nontreated cells.

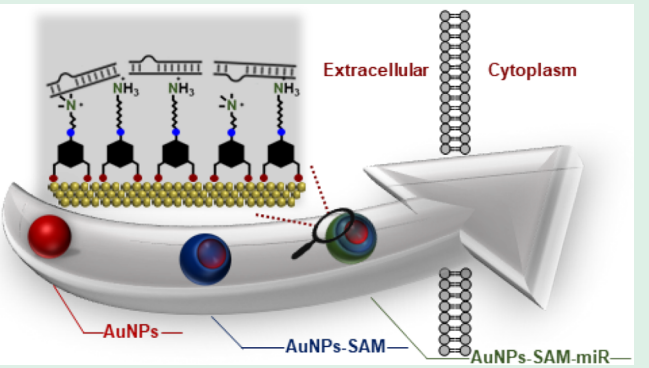

KEYWORDS: *monolayer-coated gold nanoparticles, oligonucleotides, unmodified microRNA, ammonium-terminated gold nanoparticles, transfection of miRNA*

INTRODUCTION

MicroRNAs (miRNA) are short, ∼22 nucleotides long, endogenous noncoding RNAs that can play a regulatory role by targeting messenger RNAs (mRNAs) for cleavage or translation repression.[1,2] MicroRNAs regulate complex cellular processes, and deregulation of microRNAs can lead to various diseases.[3] Given their crucial role in post-transcriptional regulation, miRNAs are often referred to as cellular fine-tuners, shaping cellular responses. Research has shown that the introduction of tumor-suppressor microRNAs can limit cancer development and progression.[4] MicroRNAs are highly unstable molecules; therefore, robust systems to deliver functional miRNAs into living cells are much needed.[5] While the therapeutic potential of miRNAs is vast, achieving targeted, efficient, and stable delivery remains the foremost hurdle, underscoring the need for advanced delivery systems.

MicroRNAs have emerged as a promising therapeutic avenue for resensitizing oncogenic pathways.[6−9] However, their therapeutic efficacy is significantly impeded by low cellular uptake and degradation during passive circulation.[9] To address this critical challenge, extensive research has focused on developing efficient gene carrier systems, such as viral and nonviral carriers.

Viral vectors, including adenoviruses, lentiviruses, and retroviruses, have demonstrated remarkable efficiency in transfection.[10−12] While viral vectors have been shown to be efficient, long-term safety, large-scale production, and potential recombination events pose significant challenges. However, their immunogenicity and the difficulties associated with their preparation have led to a growing interest in nonviral delivery systems.[10−12] Nonviral carriers, particularly liposomes, have garnered attention as promising alternatives to viral vectors in gene delivery due to their reduced immunogenicity and enhanced cellular membrane interaction.[10−13] However, these carriers are often plagued by suboptimal transfection efficiency and elevated toxicity.[10−13]

Recent studies have highlighted the potential of nonviral carriers, utilizing noble metal nanoparticles, as a promising alternative for miRNA delivery due to their ability to deliver high payloads with minimal toxicity, rendering them a favorable candidate for efficient delivery.[10,11] The advantage of noble metal nanoparticles lies not just in their delivery efficiency but also in their potential for multifunctionality—enabling simultaneous therapeutic delivery, imaging, and even triggered release upon exposure to external stimuli. As such,

Received: September 19, 2023
Revised: November 16, 2023
Accepted: November 19, 2023
Published: December 22, 2023

https://doi.org/10.1021/acsabm.3c00837
ACS Appl. Bio Mater. 2024, 7, 230−237

Scheme 1. Synthetic Route Used to Prepare the AuNPs-SAM-miR Nanoparticles

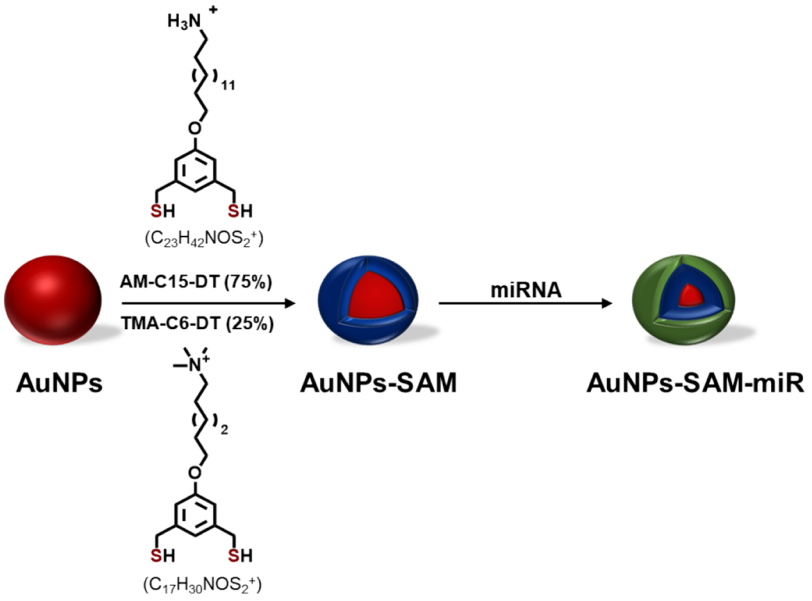

they have garnered significant attention as promising alternatives for gene delivery applications. Nonetheless, these carriers require modification with adsorbates to impart specific properties, and their cellular uptake is significantly influenced by factors such as size and charge.[11,14]

The cellular uptake of nanoparticles is strongly influenced by their size and charge. Research has shown that spherical gold nanoparticles with a core size of 50 nm or less are most effective in being taken up into cells through endocytosis.[14] Furthermore, positively charged gold nanoparticles have been found to be internalized more efficiently than negatively charged or neutral ones.[15] The attractive electrostatic forces between the positively charged gold nanoparticles and the negatively charged cell membrane allow the gold nanoparticles to disrupt the charge distribution of the cell membrane and facilitate their internalization into cells.[16]

Nanoparticle surface modification via self-assembled monolayers (SAMs) has gained widespread adoption in recent years due to the ease of formation facilitated by the binding of adsorbates to a range of noble metals including copper, gold, palladium, and silver as well as the resulting stability through the customization of interfacial properties.[17,18] The SAM moiety comprises three critical elements: the headgroup, spacer, and tailgroup, with the headgroup selection (e.g., phosphonate,[19,20] silane,[19] or thiol[17,18,21]) dependent on the substrate of interest. The spacer, typically composed of an alkyl chain, controls SAM film packing via van der Waals interactions.[22] Finally, the terminal tailgroup, typically functionalized for biomolecule conjugation, plays a pivotal role in customizing SAMs for biological applications, with common tailgroups including amines and carboxylic acids.[23] Gold, with its biocompatibility and inertness, has emerged as a particularly promising substrate for such applications.[23,24]

The physisorption of miRNA offers a more bioreactive method of immobilizing miRNA over conventional modification methods that covalently bind oligonucleotides. Unmodified miRNA can be efficiently delivered into cells through the use of gold nanoparticles functionalized with cysteamine.[25] Despite its demonstrated success, this method fails to achieve long-term stability and possibly gives rise to the deprotonation of the protonated cysteamine with slight environmental changes in pH, thereby hindering the electrostatic interactions between the miRNA and the gold nanoparticles.[26] Separately, chemisorption of chemically altered miRNA bearing a thiol moiety has been found to hinder biofunctionality by off-targeting the oligonucleotides.[27]

On the other hand, physisorption of miRNA onto SAM-decorated nanoparticles via custom-designed SAM terminal groups (e.g., amines, quaternary ammoniums, and polyethylenimines) presents a viable pathway for miRNA to adhere to these surfaces through electrostatic interactions without the need for modifying the nucleic acids of the miRNA. MicroRNAs are composed of nitrogen bases consisting of heterocyclic pyridine and/or pyrimidine structures. The nitrogen bases are glycosidically bonded to the C-1′ position of the ribose sugar, which offers a platform for the formation of nucleic acid phosphodiester bonds between the ribose sugar C-3′ and C-5′ positions and the adjacent phosphate groups.[28] The phosphate backbone provides a platform for ionic interactions between the charged adsorbates and the miRNAs.[29] The immobilization of miRNAs onto the surface leads to the oligonucleotides adopting an orientation that minimizes repulsion between the phosphate backbones; this repulsion leads to miRNAs adopting a random orientation during the immobilization process on the surface.

Our research describes a new delivery platform that specifically tackles the challenges associated with the delivery of unmodified miRNA. The use of SAMs on gold nanoparticles allows for a more targeted approach, reducing the likelihood of off-target effects of modified miRNA typically required in nanoparticle-based miRNA delivery platforms. The use of quaternary ammonium and ammonium terminal groups on the nanoparticle surface is a key feature of our methodology, providing a platform for electrostatic interactions with miRNA. This method facilitates an effective binding process that requires no alterations to the miRNA structure, thereby preserving its integrity and functionality. Our approach aims to provide a reliable alternative to conventional methods, which often compromise the stability and specificity of miRNA. Herein, we demonstrate the development of a monolayer-

https://doi.org/10.1021/acsabm.3c00837
ACS Appl. Bio Mater. 2024, 7, 230−237

coated gold nanoparticle delivery platform, **AuNPs-SAM-miR**, that can overcome cellular membrane barriers. To deliver negatively charged and hydrophilic miRNA, the system must overcome a negatively charged extracellular membrane.[30,31] To sequester the negative charges of the miRNA present in the phosphate backbones, the use of a gold nanocomplex functionalized with a mixed interface consisting of 6-(3,5-bis(mercaptomethyl)phenoxy)-*N*,*N*,*N*-trimethylhexan-1-aminium (**TMA-C6-DT**) and 15(3,5-bis(mercaptomethyl)-phenoxy)pentadecan-1-ammonium (**AM-C15-DT**) to achieve a net positive charge was pursued (Scheme 1).[32,33] The use of a quaternary ammonium terminus of **TMA-C6-DT** offers the flexibility of having a positively charged species, regardless of any moderate changes in pH. Furthermore, the ammonium terminus of **AM-C15-DT** on the gold nanoparticle surface is present for the purpose of allowing the nanoparticle complex to elute out of the lysosome once internalized into the cells.[34,35] The presence of the ammonium-termini on the nanoparticle complex hinders the acidifying process in the lysosome compartment due to the protonation of the terminal amine in the adsorbate, leading to a "proton sponge" behavior, which will inhibit degradation.[34,35] The mechanism by which the proton sponge effect inhibits degradation is not well understood, but the most highly accepted mechanism involves the high influx of ions into the endosome. The entry of Cl^- into the endosome likely disrupts the electrostatic interaction between miRNA and the ammonium termini, leading to their dissociation.[36−38] Simultaneously, the influx of ions causes a hypotonic condition that leads to the rupture of the endosome and subsequent release of its contents into the cytosol.[34,35,39]

The release of its contents into the cytosol initiates a gene regulatory process within the cell. Overall, the development of the present monolayer-coated nanoparticle system offers the capability to overcome intercellular barriers. By navigating these barriers and optimizing delivery, our system has the potential to significantly impact miRNA therapeutics by offering a tangible methodology to address long-standing challenges in this domain.

EXPERIMENTAL SECTION

A comprehensive description of the materials, methodology, and instrumentation used to synthesize the monolayer-coated gold nanoparticles is provided in the Supporting Information. In addition, descriptions of the characterization of the monolayer-coated gold nanoparticles using UV−vis spectroscopy, dynamic light scattering (Figure S2), zeta potential (Figure S3), gel mobility shift assay (Table S1 and Figure S1), XPS, and TEM are included in the Supporting Information. The synthesis of the adsorbates **TMA-C6-DT** and **AM-C15-DT** was described previously.[33]

RESULTS AND DISCUSSION

Size, Morphology, Physical Properties, and Chemical Composition of the Monolayer-Coated Gold Nanoparticles. *Hydrodynamic Diameter via Dynamic Light Scattering.* As part of the characterization of our gold nanoparticle-based delivery system, we measured the hydrodynamic diameters of the nanoparticles and functionalized nanoparticles by dynamic light scattering (DLS). This technique allows for a meaningful insight into the particle dimensions,[40,41] including contributions from the surrounding organic species.[40,41] The hydrodynamic diameters of the AuNPs, AuNPs-SAM, and AuNPs-SAM-miR species are shown in Figure 1 and Figure S2. The hydrodynamic size

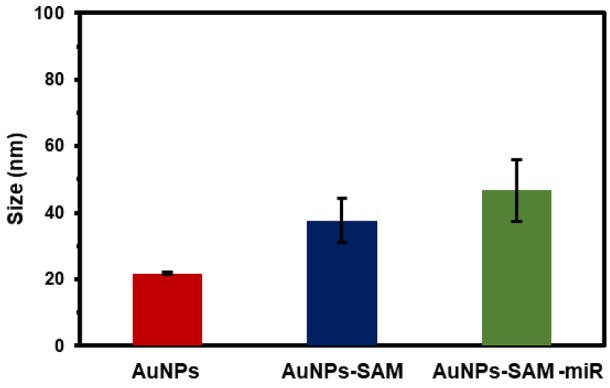

Figure 1. Hydrodynamic diameters of the AuNPs, AuNPs-SAM, and AuNPs-SAM-miR species, indicating average values of ∼22, ∼38, and ∼47 nm, respectively. The error bars represent the standard deviation of three separate measurements.

measurements of the AuNPs indicate a diameter of ∼22 nm. Upon ligand exchange between the citrate-capped AuNPs and our adsorbate mixture, the hydrodynamic size increased from ∼22 to ∼38 nm.[42] Moreover, a further increase in hydrodynamic diameter was observed after immobilization of the miRNA, showing an increase from ∼38 to ∼47 nm. The systematic increases in the hydrodynamic diameters of the nanoparticles are consistent with the formation of monolayer-coated gold nanoparticles followed by the adsorption of the miRNA moieties.

Morphological Structure and Size by TEM. The monolayer-coated gold nanoparticle complex was further subjected to transmission electron microscope (TEM) imaging to provide information about the morphology, shape, and size of the complex.[42,43] The diameter of the AuNPs is ∼17 nm with a spherical shape (Figure 2a). It should be noted that the size and morphology of the AuNP core were not affected by ligand exchange (Figure 2b) or immobilization of the miRNA (Figure 2c). The size obtained using TEM is substantially less than the size obtained by DLS. However, the former technique takes into account the interfacial double layer surrounding the metal core, whereas the latter only accounts for the particle core.[44]

Surface Charge of the Monolayer-Coated Gold Nanoparticles by Zeta (ζ) Potential. The ζ-potential analysis of the layered gold nanoparticle complex, shown in Figure 3, offers beneficial clues into the overall stability of the complex as well as the charge of the solid−liquid interface.[45] The ζ-potential value of citrate-capped AuNPs is considered stable within the range of −10.0 to −20.0 mV.[46,47] The values are dictated by the amount of negatively charged species present from the citrate capping agent, which surrounds the diffusion layer of the particle.[48]

A ζ-potential value of −11.0 mV can be observed for the AuNPs (Figure S3A), which is likely due to the minimum amount of citrate surrounding the AuNPs. From prior literature studies, AuNPs expressing a ζ-potential between −15.0 and −11.0 mV have been demonstrated to be relatively stable for several months.[49,50]

A ζ-potential value of +42.0 mV (Figure S3B) was observed after coating the AuNPs with the adsorbates (**AM-C15-DT** and **TMA-C6-DT**). The shift in the value is likely due to the positively charged termini of the adsorbate on the surface of the AuNPs. Adsorbates bearing a thiol headgroup with a positively charged tailgroup have been shown to displace

https://doi.org/10.1021/acsabm.3c00837
ACS Appl. Bio Mater. 2024, 7, 230−237

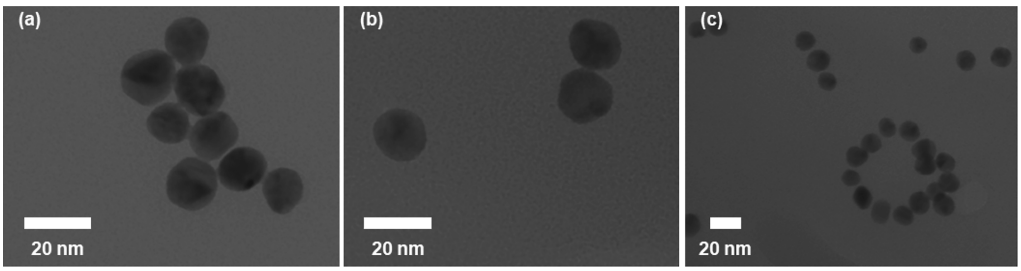

Figure 2. Transmission electron microscope images of (a) AuNPs, (b) AuNPs-SAM, and (c) AuNPs-SAM-miR.

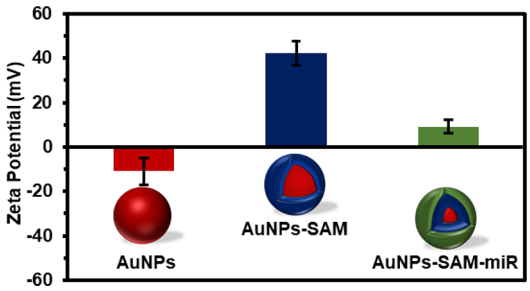

Figure 3. ζ-Potential of AuNPs, AuNPs-SAM, and AuNPs-SAM-miR.

citrate from the surrounding gold surface of the nanoparticle, forming a covalent Au−S bond.[51] Furthermore, particles decorated with positively charged tailgroups have also been documented within the literature to express a positive ζ-potential value.[51]

Incorporating the third layer in the AuNPs-SAM-miR complex decreases the ζ-potential value to +9.0 mV (Figure S3C). Coating of gold nanoparticles with nucleic acid has been documented to decrease the ζ-potential of positively charged AuNPs.[52,53] The lower value obtained might be due to sequestering of the charged surface caused by the electrostatic interaction between the termini of the ligands and the negatively charged phosphate backbone of the miRNA.

Measurement by Ultraviolet−Visible Spectroscopy. Gold nanoparticles possess a unique optical property known as surface plasmon resonance (SPR), the maximum dipole oscillation of the conduction band electrons caused by the absorption of incident light on the metal surface.[54] The strong absorption of the incident light by SPR can be measured using a UV−vis spectrophotometer.[54] The location of the SPR peak is dependent on the nanoparticle size,[55] shape,[56] nucleotides,[52] and bound ligand.[57] Figure 4 shows the SPR peaks of our nanoparticle complexes at various stages. The SPR peak (λ_{max}) of the AuNPs appears at ∼519 nm (Figure 4a), in accordance with the literature for an ∼15−20 nm gold nanoparticle.[58] The chemisorption of the adsorbates onto the AuNPs, the AuNPs-SAM, caused a red-shift in the SPR peak from 519 to 527 nm (Figure 4b). The coating of the miRNA to the nanoparticle, the AuNPs-SAM-miR, further red-shifted the SPR to 532 nm (Figure 4c).

The shifts in the SPR of our nanoparticle complexes suggest that the AuNP surface is modified. It is known that the chemisorption of the thiol onto the gold nanoparticle leads to a disruption of the electron charge density of the outer surface, causing an increase in the SPR wavelength.[57] Furthermore, the broadening of the SPR peak can be observed from our AuNPs-SAM, compared to AuNPs, due to the phenomenon called SPR damping, in which the Au−S bond causes an increase in electron conduction on the AuNP surface.[59] The shifting to a higher λ_{max} after the introduction of miRNA (Figure 4c) is potentially caused by the change in the dielectric layer around the AuNPs due to the increase in the particle thickness and the refractive index.[60,61]

Further approximation of the AuNP particle size by UV−vis was performed using the Haiss equation (eq 1)[55]

$$d = \exp\left(B_1 \frac{A_{spr}}{A_{450}} - B_2\right) \quad (1)$$

Here, d denotes the diameter of the gold nanoparticles with a deviation of approximately 11%.[55] The absorbance at the λ_{max} of the AuNPs is represented by A_{spr}, which is 0.934. Furthermore, A_{450} represents the absorbance of the AuNPs at the wavelength of 450 nm, which is 0.559. Moreover, B_1 and B_2 are determinate values provided by Haiss experiments, which are 3.00 and 2.20, respectively.[55] Based on the Haiss equation, the diameter is approximately 17 nm for the gold nanoparticle, which is similar to the TEM value.

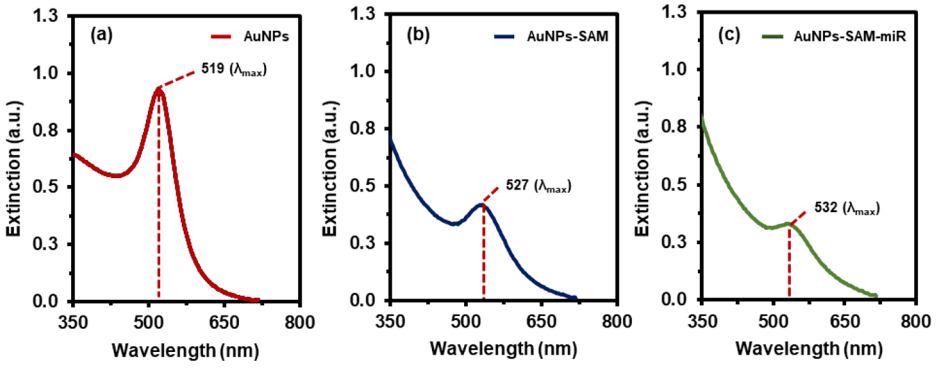

Figure 4. UV−vis spectra for (a) AuNPs, (b) AuNPs-SAM, and (c) AuNPs-SAM-miR.

https://doi.org/10.1021/acsabm.3c00837
ACS Appl. Bio Mater. 2024, 7, 230−237

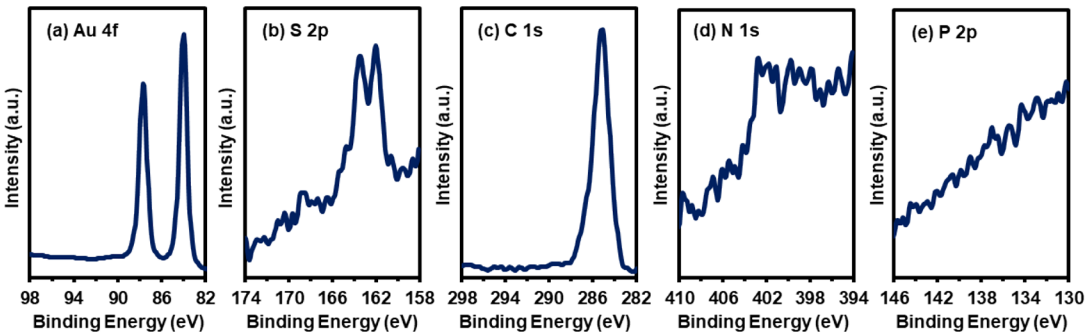

Figure 5. XPS spectra of (a) Au 4f, (b) S 2p, (c) C 1s, (d) N 1s, and (e) P 2p regions after the chemisorption of the **TMA-C6-DT** and **AM-C15-DT** adsorbates to the gold nanoparticles.

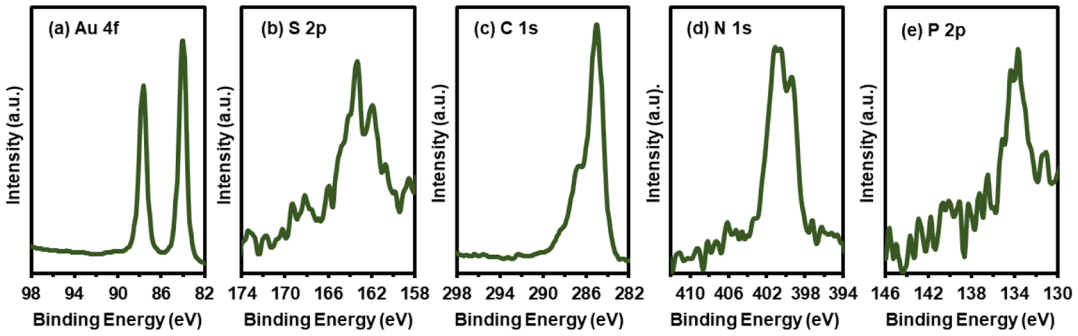

Figure 6. XPS spectra of (a) Au 4f, (b) S 2p, (c) C 1s, (d) N 1s, and (e) P 2p regions after conjugation of miRNA onto the SAMs of the gold nanoparticles.

Chemical Composition Studies by X-ray Photoelectron Spectroscopy (XPS). The chemical composition of AuNPs-SAM was examined by XPS. Figure 5 shows the high-resolution XPS spectra of the Au 4f, S 2p, C 1s, N 1s, and P 2p core electrons for the AuNPs-SAM. Note that the binding energy (BE) of the Au $4f_{7/2}$ electrons was used as a reference for all spectra obtained and was adjusted to 84 eV. The presence of a doublet in the Au region (Figure 5a), corresponding to the Au $4f_{5/2}$ and Au $4f_{7/2}$ electrons, is a signature of the Au nanoparticles.[62] The presence of a doublet in the S 2p region confirms the chemisorption of the thiol headgroup to the gold substrate after the initial ligand exchange. According to a previous literature study, the S $2p_{1/2}$ peak of a bound thiolate has a BE of ∼162 eV.[63] For an unbound thiolate, the S $2p_{3/2}$ has a BE of ∼164 eV.[32] Inspection of the S 2p region of the AuNPs-SAM (Figure 5b) confirms that the thiol was predominantly bound to the gold nanoparticles. Analysis of the C 1s region (Figure 5c) shows the presence of the hydrocarbons at BE values of ∼285 and ∼286 eV, corresponding to the C−O and C−N species, respectively.[64,65] Examination of the N 1s region (Figure 5d) exhibits two distinct peaks at ∼403 and ∼399 eV, confirming the presence of the amine termini and quaternary ammonium termini, respectively.[65,66] The P 2p region was probed as a reference for the presence of phosphate, which indicated no peaks in the region (Figure 5e).[32,33,67]

A detailed surface elemental composition of AuNPs-SAM-miR was performed to confirm the miRNA conjugation to the nanoparticle. The high-resolution spectra of the Au 4f, S 2p, C 1s, N 1s, and P 2p regions are shown in Figure 6. Figure 6a shows the signature doublet of the Au 4f region. Assessment of the S 2p region (Figure 6b), specifically the S $2p_{1/2}$ and S $2p_{3/2}$ peaks, shows a shift of the S $2p_{3/2}$ peak to a higher BE. The introduction of the miRNA could have diminished the van der Waals interactions between the alkyl chains, which likely causes a decrease in the interchain stabilization of the SAMs.[31] The C 1s region (Figure 6c) shows peaks at BE values of 285 eV (hydrocarbons), 286 eV (C−O and C−N), 287.8 (N−C−O), and 289 eV (N−C═O).[64,68] Furthermore, analysis of the N 1s region (Figure 6d) shows a distinct peak at ∼400 eV that originates from the amide heterocycles (purine and pyrimidine) in the miRNA.[68,69] Additionally, analysis of the P 2p region (Figure 6e) shows a newly developed peak at a BE of ∼133 eV, originating from the phosphate backbone of the miRNA.[68,69] Altogether, the elemental composition analysis by XPS, in conjunction with DLS, UV−vis, and ζ-potential values, supports the successful formation of our AuNPs-SAM-miR nanoparticle complex.

Measurement of the miRNA in HOS cells by a Quantitative Polymerase Chain Reaction (qPCR). To evaluate whether our AuNPs-SAM-miR were internalized and delivered its cargo into host cells, we transfected HOS cells with our nanoparticles and measured the delivered miRNA using the qPCR technique. Cells were transfected with AuNPs-SAM, scrambled RNA oligomer-loaded (AuNPs-SAM-NC) as a negative control, or miR-509-3p*-loaded nanoparticle complex (AuNPs-SAM-miR), along with nontreated cells (NT). We selected miR-509-3p for this study because it has been shown that miR-509-3p is downregulated in osteosarcoma, and overexpression of miR-509-3p inhibits HOS cell metastasis and sensitizes HOS cells to Cisplatin.[70] After 24 h of incubation, total RNA was extracted and quantified. The miR-509-3p levels were then measured with the TaqMan miRNA reverse transcription kit for HSA-miR-509-3p according to the manufacturer's instructions. Figure 7 shows the relative miR-509-3p levels in each group from three separate experiments.

https://doi.org/10.1021/acsabm.3c00837
ACS Appl. Bio Mater. 2024, 7, 230−237

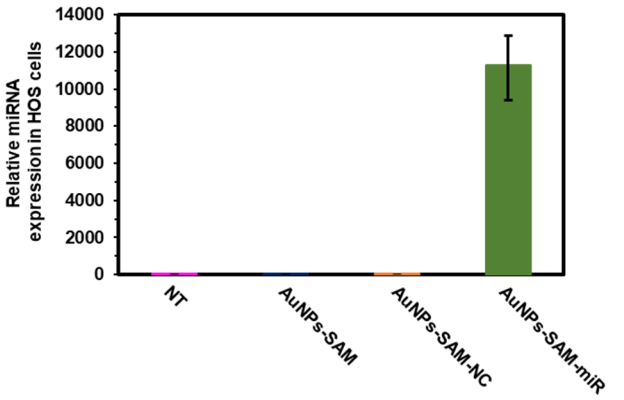

Figure 7. Relative miR-509-3p level in nontreated (NT) and AuNPs-SAM-, AuNPs-SAM-NC-, and AuNPs-SAM-miR-treated HOS cell lines measured by Taqman PCR.

The miRNA level in HOS cell lines treated with AuNPs-SAM-miR was ∼11,268-fold higher compared to nontreated, AuNPs-SAM-treated, or AuNPs-SAM-NC-treated cells.

CONCLUSIONS

The gold nanoparticles served as a substrate for the chemisorption of the adsorbates and further provided termini essential for electrostatic immobilization of the miRNA. Furthermore, the selected ligand mixture used to displace the citrate capping agent of the gold nanoparticle was capable of simultaneously stabilizing the nanoparticle complex. The choice of the ligand mixture was selected not only for colloidal stabilization but also for specific electrostatic and structural features that facilitate the binding of unmodified miRNA, which is crucial for mitigating off-target effects commonly associated with modified miRNAs that are required in existing nanoparticle-based delivery platforms. The layered gold nanoparticle complex was characterized by UV−vis, DLS, TEM, ζ-potential, and XPS. The ability of the nanoparticle complex to deliver miRNA-509-3p into the HOS cells was measured by qPCR. The qPCR analysis showed an ∼11,268-fold increase in miRNA levels compared to the controls. Overall, we have demonstrated the successful delivery of miRNA into cells and the subsequent release of its payload into the cellular cytosol. The increase in miRNA levels within the cells treated with AuNPs-SAM-miR not only substantiates the effective delivery and release of miRNA payloads into the cell but also suggests that our nanoparticle system offers a general strategy for transporting miRNA into cells. Further development and *in vivo* validation are needed to establish whether this promising system can be used to correct miRNA dysregulation.

This achievement stands as a major advancement in nanoparticle-based unmodified miRNA delivery systems. Specifically, the efficiency of our approach, corroborated by qPCR results, offers a substantive advance in the delivery of unmodified miRNA. Extending beyond miRNA, the robustness of our platform is promising for other gene-therapy applications. Its potential to deliver unmodified nucleic acids such as DNA, siRNA, and mRNA positions it as a versatile tool to treat diverse genetic disorders.

As an alternative delivery vector to existing nanoparticle-based platforms that require modified miRNAs, our system overcomes significant challenges that have historically impeded the robust delivery of miRNA. Through the incorporation of positively charged SAM-coated gold nanoparticles, our strategy directly addresses the issues of miRNA off-target effects, circumventing the need for direct miRNA modification. The novel application of charged terminal groups on SAM-coated nanoparticles, specifically ammonium and quaternary ammonium groups, offers a high-precision delivery method while preserving the structural and functional integrity of the delivered miRNA.

ASSOCIATED CONTENT

Supporting Information

The Supporting Information is available free of charge on the ACS Publications Web site at DOI The Supporting Information is available free of charge at https://pubs.acs.org/doi/10.1021/acsabm.3c00837.

Experimental section, synthesis of a layer−by−layer Au nanoparticle complex (Table S1: preparation of AuNPs−SAM−miR conjugates and Figure S1: gel mobility assay), characterization of the nanocomplex (Figure S2: DLS size distribution and Figure S3: zeta potential analysis), and transfection of AuNPs−SAM−miR into human osteosarcoma cells (PDF)

AUTHOR INFORMATION

Corresponding Authors

Preethi H. Gunaratne − *Department of Biology and Biochemistry, University of Houston, Houston, Texas 77204−5001, United States*; Email: phgunaratne@uh.edu

T. Randall Lee − *Departments of Chemistry and Chemical Engineering and the Texas Center for Superconductivity, University of Houston, Houston, Texas 77204−5003, United States*; orcid.org/0000-0001-9584-8861; Email: trlee@uh.edu

Authors

Johnson Hoang − *Department of Biology and Biochemistry, University of Houston, Houston, Texas 77204−5001, United States*

Sagar L. Patil − *Department of Biology and Biochemistry, University of Houston, Houston, Texas 77204−5001, United States; St. Jude Children's Research Hospital, Memphis, Tennessee 38105, United States*

Pannaree Srinoi − *Departments of Chemistry and Chemical Engineering and the Texas Center for Superconductivity, University of Houston, Houston, Texas 77204−5003, United States; Department of Chemistry and Centre of Excellence for Innovation in Chemistry, Faculty of Science, Kasetsart University, Bangkok 10900, Thailand*; orcid.org/0000-0003-4400-468X

Tingting Liu − *Departments of Chemistry and Chemical Engineering and the Texas Center for Superconductivity, University of Houston, Houston, Texas 77204−5003, United States*

Maria D. Marquez − *Departments of Chemistry and Chemical Engineering and the Texas Center for Superconductivity, University of Houston, Houston, Texas 77204−5003, United States*

Orawan Khantamat − *Department of Biochemistry, Faculty of Medicine, Chiang Mai University, Chiang Mai 50200, Thailand*; orcid.org/0000-0003-1328-3049

https://doi.org/10.1021/acsabm.3c00837
ACS Appl. Bio Mater. 2024, 7, 230−237

Wirote Tuntiwechapikul − *Department of Biochemistry, Faculty of Medicine, Chiang Mai University, Chiang Mai 50200, Thailand;* orcid.org/0000-0003-1365-476X

Complete contact information is available at: https://pubs.acs.org/10.1021/acsabm.3c00837

Notes

The authors declare no competing financial interest.

■ ACKNOWLEDGMENTS

We thank the National Science Foundation (CHE-2109174, T.R.L.), the Robert A. Welch Foundation (grant no. E-1320, T.R.L.), and the Cancer Prevention and Research Institute of Texas (RP110355; P.G.) for generous financial support.

■ REFERENCES

(1) Bartel, D. P. MicroRNAs: genomics, biogenesis, mechanism, and function. *Cell* **2004**, *116* (2), 281−97.
(2) Saini, V.; Dawar, R.; Suneja, S.; Gangopadhyay, S.; Kaur, C. Can microRNA become next-generation tools in molecular diagnostics and therapeutics? A systematic review. *EJMHG* **2021**, *22* (1), 4.
(3) Garzon, R.; Marcucci, G.; Croce, C. M. Targeting microRNAs in cancer: rationale, strategies and challenges. *Nat. Rev. Drug Discovery* **2010**, *9* (10), 775−89.
(4) Otmani, K.; Lewalle, P. Tumor Suppressor miRNA in Cancer Cells and the Tumor Microenvironment: Mechanism of Deregulation and Clinical Implications. *Front. Oncol.* **2021**, *11*, No. 708765, DOI: 10.3389/fonc.2021.708765.
(5) Bravo, V.; Rosero, S.; Ricordi, C.; Pastori, R. L. Instability of miRNA and cDNAs derivatives in RNA preparations. *Biochem. Biophys. Res. Commun.* **2007**, *353* (4), 1052−1055.
(6) Chakraborty, C.; Sharma, A. R.; Sharma, G.; Sarkar, B. K.; Lee, S.-S. The novel strategies for next-generation cancer treatment: miRNA combined with chemotherapeutic agents for the treatment of cancer. *Oncotarget* **2018**, *9* (11), 10164−10174.
(7) Mognato, M.; Celotti, L. MicroRNAs Used in Combination with Anti-Cancer Treatments Can Enhance Therapy Efficacy. *Mini Rev. Med. Chem.* **2015**, *15* (13), 1052−1062.
(8) Li, H.; Yang, B. B. Friend or foe: the role of microRNA in chemotherapy resistance. *Acta Pharmacol. Sin.* **2013**, *34* (7), 870−879.
(9) Reda El Sayed, S.; Cristante, J.; Guyon, L.; Denis, J.; Chabre, O.; Cherradi, N. MicroRNA Therapeutics in Cancer: Current Advances and Challenges. *Cancers (Basel)* **2021**, *13* (11), 2680.
(10) Yang, N. An overview of viral and nonviral delivery systems for microRNA. *Int. J. Pharm. Investig.* **2015**, *5* (4), 179−181.
(11) Jin, L.; Zeng, X.; Liu, M.; Deng, Y.; He, N. Current Progress in Gene Delivery Technology Based on Chemical Methods and Nano-carriers. *Theranostics* **2014**, *4* (3), 240−255.
(12) Dasgupta, I.; Chatterjee, A. Recent Advances in miRNA Delivery Systems. *Methods Protoc.* **2021**, *4* (1), 10.
(13) Zhi, D.; Zhang, S.; Wang, B.; Zhao, Y.; Yang, B.; Yu, S. Transfection Efficiency of Cationic Lipids with Different Hydrophobic Domains in Gene Delivery. *Bioconj. Chem.* **2010**, *21* (4), 563−577.
(14) Chithrani, B. D.; Ghazani, A. A.; Chan, W. C. W. Determining the Size and Shape Dependence of Gold Nanoparticle Uptake into Mammalian Cells. *Nano Lett.* **2006**, *6* (4), 662−668.
(15) Foroozandeh, P.; Aziz, A. A. Insight into Cellular Uptake and Intracellular Trafficking of Nanoparticles. *Nanoscale Res. Lett.* **2018**, *13* (1), 339.
(16) Nangia, S.; Sureshkumar, R. Effects of Nanoparticle Charge and Shape Anisotropy on Translocation through Cell Membranes. *Langmuir* **2012**, *28* (51), 17666−17671.
(17) Vericat, C.; Vela, M.; Corthey, G.; Pensa, E.; Cortés, E.; Fonticelli, M.; Ibanez, F.; Benitez, G.; Carro, P.; Salvarezza, R. Self-Assembled Monolayers of Thiolates on Metals: A Review Article on Sulfur-Metal Chemistry and Surface Structures. *RSC Adv.* **2014**, *4*, 27730.
(18) Ielo, I.; Rando, G.; Giacobello, F.; Sfameni, S.; Castellano, A.; Galletta, M.; Drommi, D.; Rosace, G.; Plutino, M. R. Synthesis, Chemical−Physical Characterization, and Biomedical Applications of Functional Gold Nanoparticles: A Review. *Mol.* **2021**, *26* (19), 5823.
(19) Haensch, C.; Hoeppener, S.; Schubert, U. S. Chemical modification of self-assembled silane based monolayers by surface reactions. *Chem. Soc. Rev.* **2010**, *39* (6), 2323−2334.
(20) Bauer, T.; Schmaltz, T.; Lenz, T.; Halik, M.; Meyer, B.; Clark, T. Phosphonate- and Carboxylate-Based Self-Assembled Monolayers for Organic Devices: A Theoretical Study of Surface Binding on Aluminum Oxide with Experimental Support. *ACS Appl. Mater. & Interfaces* **2013**, *5* (13), 6073−6080.
(21) Vericat, C.; Vela, M. E.; Benitez, G.; Carro, P.; Salvarezza, R. C. Self-assembled monolayers of thiols and dithiols on gold: new challenges for a well-known system. *Chem. Soc. Rev.* **2010**, *39* (5), 1805−1834.
(22) Love, J. C.; Estroff, L. A.; Kriebel, J. K.; Nuzzo, R. G.; Whitesides, G. M. Self-Assembled Monolayers of Thiolates on Metals as a Form of Nanotechnology. *Chem. Rev.* **2005**, *105* (4), 1103−1170.
(23) Samanta, D.; Sarkar, A. Immobilization of bio-macromolecules on self-assembled monolayers: methods and sensor applications. *Chem. Soc. Rev.* **2011**, *40* (5), 2567−2592.
(24) Shukla, R.; Bansal, V.; Chaudhary, M.; Basu, A.; Bhonde, R. R.; Sastry, M. Biocompatibility of Gold Nanoparticles and Their Endocytotic Fate Inside the Cellular Compartment: A Microscopic Overview. *Langmuir* **2005**, *21* (23), 10644−10654.
(25) Ghosh, R.; Singh, L. C.; Shohet, J. M.; Gunaratne, P. H. A gold nanoparticle platform for the delivery of functional microRNAs into cancer cells. *Biomater.* **2013**, *34* (3), 807−816.
(26) Lee, S.-H.; Lin, W.-C.; Kuo, C.-H.; Karakachian, M.; Lin, Y.-C.; Yu, B.-Y.; Shyue, J.-J. Photooxidation of Amine-Terminated Self-Assembled Monolayers on Gold. *J. Phys. Chem. C* **2010**, *114* (23), 10512−10519.
(27) Jackson, A. L.; Burchard, J.; Leake, D.; Reynolds, A.; Schelter, J.; Guo, J.; Johnson, J. M.; Lim, L.; Karpilow, J.; Nichols, K.; Marshall, W.; Khvorova, A.; Linsley, P. S. Position-specific chemical modification of siRNAs reduces "off-target" transcript silencing. *RNA* **2006**, *12* (7), 1197−1205.
(28) Ra; rsquo; ed, A.-K.; Rosni, A. A Survey of Compute Intensive Algorithms for Ribo Nucleic Acids Structural Detection. *J. Comp. Sci.* **2009**, *5* (10), 680 DOI: 10.3844/jcssp.2009.680.689.
(29) Ding, Y.; Jiang, Z.; Saha, K.; Kim, C. S.; Kim, S. T.; Landis, R. F.; Rotello, V. M. Gold nanoparticles for nucleic acid delivery. *Mol. Ther.: the journal of the American Society of Gene Therapy* **2014**, *22* (6), 1075−1083.
(30) Yang, Y.; Sunoqrot, S.; Stowell, C.; Ji, J.; Lee, C.-W.; Kim, J. W.; Khan, S. A.; Hong, S. Effect of Size, Surface Charge, and Hydrophobicity of Poly(amidoamine) Dendrimers on Their Skin Penetration. *Biomacromolecules* **2012**, *13* (7), 2154−2162.
(31) Gupta, R.; Rai, B. Effect of Size and Surface Charge of Gold Nanoparticles on their Skin Permeability: A Molecular Dynamics Study. *Sci. Rep.* **2017**, *7* (1), 45292.
(32) Hoang, J.; Park, C. S.; Lee, H. J.; Marquez, M. D.; Zenasni, O.; Gunaratne, P. H.; Lee, T. R. Quaternary Ammonium-Terminated Films Formed from Mixed Bidentate Adsorbates Provide a High-Capacity Platform for Oligonucleotide Delivery. *ACS Appl. Mater. Interfaces* **2018**, *10* (47), 40890−40900.
(33) Hoang, J.; Park, C. S.; Marquez, M. D.; Gunaratne, P. H.; Lee, T. R. DNA Binding on Self-Assembled Monolayers Terminated with Mixtures of Ammonium and Trimethylammonium Groups: Toward a Gene-Delivery Platform. *ACS Appl. Nano Mater.* **2020**, *3* (7), 6621−6628.
(34) Liang, W.; W. Lam, J. K.; Ceresa, B. Endosomal Escape Pathways for Non-Viral Nucleic Acid Delivery Systems. *Mol. Regul. Endocytosis* **2012**, 429−456.
(35) Creusat, G.; Rinaldi, A.-S.; Weiss, E.; Elbaghdadi, R.; Remy, J.-S.; Mulherkar, R.; Zuber, G. Proton Sponge Trick for pH-Sensitive

Disassembly of Polyethylenimine-Based siRNA Delivery Systems. *Bioconj. Chem.* **2010**, *21* (5), 994−1002.
(36) Lipfert, J.; Doniach, S.; Das, R.; Herschlag, D. Understanding nucleic acid-ion interactions. *Annu. Rev. Biochem.* **2014**, *83*, 813−841.
(37) Landry, K. A.; Sun, P.; Huang, C.-H.; Boyer, T. H. Ion-exchange selectivity of diclofenac, ibuprofen, ketoprofen, and naproxen in ureolyzed human urine. *Water Res.* **2015**, *68*, 510−521.
(38) Freeman, E. C.; Weiland, L. M.; Meng, W. S. Modeling the proton sponge hypothesis: examining proton sponge effectiveness for enhancing intracellular gene delivery through multiscale modeling. *J. Biomater. Sci. Polym. Ed.* **2013**, *24* (4), 398−416.
(39) Lee, J.; Sands, I.; Zhang, W.; Zhou, L.; Chen, Y. DNA-inspired nanomaterials for enhanced endosomal escape. *Proc. Natl. Acad. Sci. U.S.A.* **2021**, *118* (19), No. e2104511118.
(40) Jans, H.; Liu, X.; Austin, L.; Maes, G.; Huo, Q. Dynamic Light Scattering as a Powerful Tool for Gold Nanoparticle Bioconjugation and Biomolecular Binding Studies. *Anal. Chem.* **2009**, *81* (22), 9425−9432.
(41) Khlebtsov, B. N.; Khlebtsov, N. G. On the measurement of gold nanoparticle sizes by the dynamic light scattering method. *Colloid J.* **2011**, *73* (1), 118−127.
(42) Dewi, M. R.; Laufersky, G.; Nann, T. A highly efficient ligand exchange reaction on gold nanoparticles: preserving their size, shape and colloidal stability. *RSC Adv.* **2014**, *4* (64), 34217−34220.
(43) Akhtar, S.; Asiri, S. M.; Khan, F. A.; Gunday, S. T.; Iqbal, A.; Alrushaid, N.; Labib, O. A.; Deen, G. R.; Henari, F. Z. Formulation of gold nanoparticles with hibiscus and curcumin extracts induced anti-cancer activity. *Arab. J. Chem.* **2022**, *15* (2), No. 103594.
(44) Domingos, R. F.; Baalousha, M. A.; Ju-Nam, Y.; Reid, M. M.; Tufenkji, N.; Lead, J. R.; Leppard, G. G.; Wilkinson, K. J. Characterizing Manufactured Nanoparticles in the Environment: Multimethod Determination of Particle Sizes. *Environ. Sci. Technol.* **2009**, *43* (19), 7277−7284.
(45) Bhattacharjee, S. DLS and zeta potential − What they are and what they are not? *JCR* **2016**, *235*, 337−351.
(46) Patel, V.; Agrawal, Y. Nanosuspension: An approach to enhance solubility of drugs. *J. Adv. Pharm. Technol. Res.* **2011**, *2* (2), 81−87.
(47) Karimi, S.; Moshaii, A.; Nikkhah, M. Controlled synthesis of colloidal monodisperse gold nanoparticles in a wide range of sizes; investigating the effect of reducing agent. *Mater. Res. Express* **2019**, *6*, 1150f2.
(48) Jaganathan, H.; Mitra, S.; Srinivasan, S.; Dave, B.; Godin, B. Design and in vitro evaluation of layer by layer siRNA nanovectors targeting breast tumor initiating cells. *PLoS One* **2014**, *9* (4), No. e91986.
(49) Deng, H. H.; Li, G. W.; Hong, L.; Liu, A. L.; Chen, W.; Lin, X. H.; Xia, X. H. Colorimetric sensor based on dual-functional gold nanoparticles: analyte-recognition and peroxidase-like activity. *Food Chem.* **2014**, *147*, 257−261.
(50) Das, N.; Kumar, A.; Kumar Roy, S.; Kumar Satija, N.; Raja Gopal, R. Bare plasmonic metal nanoparticles: synthesis, characterisation and in vitro toxicity assessment on a liver carcinoma cell line. *IET nanobiotechnology* **2020**, *14* (9), 851−857.
(51) Arvizo, R. R.; Verma, A.; Rotello, V. M. Biomacromolecule Surface Recognition using Nanoparticle Receptors. *Supramol. Chem.* **2005**, *17* (1−2), 155−161.
(52) Elbakry, A.; Zaky, A.; Liebl, R.; Rachel, R.; Goepferich, A.; Breunig, M. Layer-by-Layer Assembled Gold Nanoparticles for siRNA Delivery. *Nano Lett.* **2009**, *9* (5), 2059−2064.
(53) Guo, J.; Armstrong, M. J.; O'Driscoll, C. M.; Holmes, J. D.; Rahme, K. Positively charged, surfactant-free gold nanoparticles for nucleic acid delivery. *RSC Adv.* **2015**, *5* (23), 17862−17871.
(54) Huang, X.; El-Sayed, M. A. Gold nanoparticles: Optical properties and implementations in cancer diagnosis and photothermal therapy. *J. Adv. Res.* **2010**, *1* (1), 13−28.
(55) Haiss, W.; Thanh, N. T. K.; Aveyard, J.; Fernig, D. G. Determination of Size and Concentration of Gold Nanoparticles from UV−Vis Spectra. *Anal. Chem.* **2007**, *79* (11), 4215−4221.
(56) Goyal, D.; Suman; Saini, G. S. S.; Kumar, R. Size and shape approximation of gold nanoparticles using theoretical modelling. *AIP Conf. Proc.* **2015**, *1675* (1), No. 030067.
(57) Zijlstra, P.; Paulo, P. M. R.; Yu, K.; Xu, Q.-H.; Orrit, M. Chemical Interface Damping in Single Gold Nanorods and Its Near Elimination by Tip-Specific Functionalization. *Angew. Chem., Int. Ed.* **2012**, *51* (33), 8352−8355.
(58) Zuber, A.; Purdey, M.; Schartner, E.; Forbes, C.; van der Hoek, B.; Giles, D.; Abell, A.; Monro, T.; Ebendorff-Heidepriem, H. Detection of gold nanoparticles with different sizes using absorption and fluorescence based method. *Sens. Actuators B: Chem.* **2016**, *227*, 117−127.
(59) Garcia, M. A.; de la Venta, J.; Crespo, P.; Llopis, J.; Penadés, S.; Fernández, A.; Hernando, A. Surface plasmon resonance of capped Au nanoparticles. *Phys. Rev. B* **2005**, *72* (24), No. 241403.
(60) Marchant, M. J.; Guzmán, L.; Corvalán, A. H.; Kogan, M. J. Gold@Silica Nanoparticles Functionalized with Oligonucleotides: A Prominent Tool for the Detection of the Methylated Reprimo Gene in Gastric Cancer by Dynamic Light Scattering. *Nanomaterials* **2019**, *9* (9), 1333.
(61) Schneider, T. W.; Buttry, D. A. Electrochemical quartz crystal microbalance studies of adsorption and desorption of self-assembled monolayers of alkyl thiols on gold. *J. Am. Chem. Soc.* **1993**, *115* (26), 12391−12397.
(62) Chenakin, S. P.; Kruse, N. Au 4f spin−orbit coupling effects in supported gold nanoparticles. *Phys. Chem. Chem. Phys.* **2016**, *18* (33), 22778−22782.
(63) Castner, D. G.; Hinds, K.; Grainger, D. W. X-ray Photoelectron Spectroscopy Sulfur 2p Study of Organic Thiol and Disulfide Binding Interactions with Gold Surfaces. *Langmuir* **1996**, *12* (21), 5083−5086.
(64) Baio, J. E.; Weidner, T.; Brison, J.; Graham, D. J.; Gamble, L. J.; Castner, D. G. Amine terminated SAMs: Investigating why oxygen is present in these films. *J. Electron Spectrosc. Relat. Phenom.* **2009**, *172* (1), 2−8.
(65) Ah Qune, L. F. N.; Makino, K.; Tamada, K.; Chen, W.; Wee, A. T. S. Selective Adsorption of l-Tartaric Acid on Gemini-Type Self-Assembled Monolayers. *J. Phys. Chem. C* **2008**, *112* (8), 3049−3053.
(66) Techane, S. D.; Gamble, L. J.; Castner, D. G. X-ray photoelectron spectroscopy characterization of gold nanoparticles functionalized with amine-terminated alkanethiols. *Biointerphases* **2011**, *6* (3), 98−104.
(67) Ptasińska, S.; Stypczyńska, A.; Nixon, T.; Mason, N. J.; Klyachko, D. V.; Sanche, L. X-ray induced damage in DNA monitored by X-ray photoelectron spectroscopy. *J. Chem. Phys.* **2008**, *129* (6), No. 065102.
(68) Gong, P.; Lee, C. Y.; Gamble, L. J.; Castner, D. G.; Grainger, D. W. Surface Coverage and Structure of Mixed DNA/Alkylthiol Monolayers on Gold: Characterization by XPS, NEXAFS, and Fluorescence Intensity Measurements. *Anal. Chem.* **2006**, *78* (10), 3326−3334.
(69) Lee, C.-Y.; Nguyen, P.-C. T.; Grainger, D. W.; Gamble, L. J.; Castner, D. G. Structure and DNA Hybridization Properties of Mixed Nucleic Acid/Maleimide−Ethylene Glycol Monolayers. *Anal. Chem.* **2007**, *79* (12), 4390−4400.
(70) Patil, S. L.; Palat, A.; Pan, Y.; Rajapakshe, K.; Mirchandani, R.; Bondesson, M.; Yustein, J. T.; Coarfa, C.; Gunaratne, P. H. MicroRNA-509−3p inhibits cellular migration, invasion, and proliferation, and sensitizes osteosarcoma to cisplatin. *Sci. Rep.* **2019**, *9* (1), 19089.

https://doi.org/10.1021/acsabm.3c00837
ACS Appl. Bio Mater. 2024, 7, 230−237